18th International Conference on Structural Mechanics in Reactor Technology (SMiRT 18)
Beijing, China, August 7-12, 2005
SMiRT18-S06-2

IMPROVEMENT OF INELASTIC CONSTITUTIVE MODEL FOR AUSTENITIC STAINLESS STEEL FOR DESIGN USE

Yukio TAKAHASHI*
Central Research Institute of Electric Power Industry
Iwado-Kita 2-11-1, Komae-shi, Tokyo, Japan
Phone: +81-3-3480-2111
Fax: +81-3-3430-2410
E-mail: yukio@criepi.denken.or.jp

Naoto KASAHARA
Japan Nuclear Cycle Development Institute,
Narita, Oarai, Ibaraki, Japan
Phone: +81-29-267-4141
Fax: +81-29-266-3675
E-mail: kasahara@oec.jnc.go.jp

Hiroshi SHIBAMOTO
Japan Atomic Power Company (dispatched to Japan Nuclear Cycle Development Institute)
Narita, Oarai, Ibaraki, Japan
Phone: +81-29-267-4141
Fax: +81-29-266-3675
E-mail: sibamoto@oec.jnc.go.jp

Kazuhiko INOUE
Japan Atomic Power Company (dispatched to Japan Nuclear Cycle Development Institute)
Narita, Oarai, Ibaraki, Japan
Phone: +81-29-267-4141
Fax: +81-29-266-3675
E-mail: inoue.kazuhiko@oec.jnc.go.jp

ABSTRACT

To prevent creep-fatigue failure or excessive deformation in high-temperature components of fast reactor plants, accurate estimation of inelastic deformation and resulting damage is essential. In performing inelastic analysis, employment of constitutive models which can precisely reproduce inelastic deformation of the material is of critical importance. The authors have been engaged in the development of inelastic constitutive model used in structural design assessment as a part of a whole structural design standard. Various improvements were made on the nonlinear hardening model proposed by Ohno and Wang, placing an emphasis on capability to simulate inelastic deformation behavior of austenitic stainless steels, under regular or irregular cyclic loading possibly with temperature variation. It was demonstrated that the model can simulate the deformation behavior under various loading conditions with a sufficient accuracy.

Keywords: Inelastic analysis, austenitic stainless steel, cyclic loading, creep, structural design

1. INTRODUCTION

Because of high thermal stress and low yield strength of structural materials, proper estimation of inelastic deformation and resulting damage is an essential task in the structural design for high-temperature components of fast reactor plants to prevent creep-fatigue failure or excessive deformation. Detailed inelastic analysis by finite element method can principally provide realistic estimates of inelastic strain and stress without too large conservatism due to simplification of geometry or material behavior. In performing detailed inelastic analysis

for the design assessment, however, employment of a proper constitutive model which can precisely reproduce inelastic deformation of the material is of critical importance.

In liquid metal-cooled fast breeder reactor (LMFBR) plants constructed or designed in the past employed austenitic stainless steels as a structural material for substantial portions of the plants including primary cooling systems. Among them, type 304 stainless steel was most widely used in older plants. Newer plants employed low-carbon nitrogen-controlled 316 stainless steel designated as 316SPH. 316L(N) in Europe or as 316FR in Japan. They show quantitatively similar deformation and failure behavior and can be treated in a similar way. Principal features of these materials in respect with deformation behavior pertaining to constitutive modeling can be summarized as:

(i) Low initial yield stress but large amount of cyclic hardening (especially at higher temperatures)
(ii) Small strain rate dependency up to the temperatures LMFBR plants are operating (i.e. 500-550C)
(iii) Relatively small ratcheting both under proportional and nonproportional loading.

The first systematic study on the inelastic constitutive model for LMFBR design application can be traced back to a series of work done by researchers in Oak Ridge National Laboratory (ORNL) (e.g. Pugh, 1983). In the so-called ORNL model, time-independent plastic strain and time-dependent creep strain are treated separately and various modifications were introduced on classical plasticity and creep models. However, due to inherent limitations of the classical models, capability of simulation is not sufficient.

Later on, Chaboche et al. (1983) in France developed plastic and visco-plastic models based on nonlinear hardening rule originally proposed by Armstrong and Frederick (1966). These models improved reproducibility of material behavior under cyclic loading significantly but still show clear deficiency when applied to the simulation of ratcheting deformation.

One of the authors has been also engaged in the development of inelastic constitutive model for austenitic stainless steels to be used in structural design assessment (Takahashi, 1993, 1998). After choosing the nonlinear kinematic hardening model proposed by Ohno and Wang (1993ab), instead of the former two-surface type model because of suitability to ratcheting analysis (Takahashi and Tanimoto, 1995), various modifications have been made placing an emphasis on capability to simulate inelastic deformation behavior of the materials under regular or irregular cyclic loading accompanied by temperature variation. Based on the requirement from the designer side, a model particularly suitable for conservative assessment of ratcheting deformation and fatigue damage assessment was also developed in addition to that corresponding to mean property of the materials. An outline of these latest models will be given in the paper.

2. CONSTITUTIVE MODELING

2.1 Modeling of Plastic Deformation

2.1.1 Plastic hardening index surface

At first, the following function is defined in inelastic strain space.

$$g = \frac{2}{3}\left(\varepsilon_{ij}^{in} - \beta_{ij}\right)\left(\varepsilon_{ij}^{in} - \beta_{ij}\right) - \rho^2 = 0 \tag{1}$$

where ε_{ij}^{in} is inelastic strain given as a sum of plastic strain, ε_{ij}^{p} and creep strain, ε_{ij}^{c}. ρ and β_{ij} are 0 before initial inelastic strain and change with inelastic strain according to the following equations:

$$\dot{\beta}_{ij} = \frac{1}{2}\nu_{ij}\dot{\varepsilon}_{kl}^{in}\nu_{kl} \tag{2}$$

$$\dot{\rho} = \frac{1}{\sqrt{6}}\nu_{ij}\dot{\varepsilon}_{ij}^{in} \tag{3}$$

$$\nu_{ij} = \frac{\partial g}{\partial \varepsilon_{ij}^{in}} \Bigg/ \sqrt{\frac{\partial g}{\partial \varepsilon_{kl}^{in}}\frac{\partial g}{\partial \varepsilon_{kl}^{in}}} = \frac{\varepsilon_{ij}^{in} - \beta_{ij}}{\sqrt{(\varepsilon_{kl}^{in} - \beta_{kl})(\varepsilon_{kl}^{in} - \beta_{kl})}} \tag{4}$$

In addition to these equations, the following resetting operation is applied:

$$\rho = 0 \tag{5}$$

$$\beta_{ij} = \varepsilon_{ij}^{in} \tag{6}$$

when

$$\nu_{ij}\dot{\varepsilon}_{ij}^{in} < 0 \tag{7}$$

is satisfied. These equations assign ρ a role of representing inelastic strain range and it is used to calculate cyclic hardening as will be shown.

2.1.2 Yield surface

Yield surface is defined in deviatoric stress space as

$$f = \frac{3}{2}\left(s_{ij} - \alpha_{ij}\right)\left(s_{ij} - \alpha_{ij}\right) - \kappa^2 = 0 \tag{8}$$

where、s_{ij} is deviatric part of stress and α_{ij} and κ represent shift and size of the surface, respectively. Changes of these parameters are usually called as kinematic and isotropic hardening, respectively.

2.1.3 Hardening rule

As a skeleton of the current model, the kinematic hardening model proposed by Ohno and Wang [5-6] is adopted. In their model, kinematic hardening is given as a sum of their subelements as

$$\alpha_{ij} = \sum_{k=1}^{n} \alpha_{ij}^{(k)} \tag{9}$$

where $\alpha_{ij}^{(k)}$ is the k-th element of a α_{ij} and *n* is the total number of elements.

All elements of $\alpha_{ij}^{(k)}$ are initially 0 for isotropic materials and develop with inelastic deformation according to the following equation;

$$\dot{\alpha}_{ij}^{(k)} = \zeta^{(k)}\left\{\frac{2}{3}r^{(k)}\dot{\varepsilon}_{ij}^{in} - H\left(\overline{\alpha^{(k)}}^2 - r^{(k)2}\right)\frac{\left\langle \dot{\varepsilon}_{kl}^{in}\alpha_{kl}^{(k)}\right\rangle}{\overline{\alpha^{(k)}}}\alpha_{ij}^{(k)} - C\alpha_{ij}^{(k)}\overline{\dot{\varepsilon}^{in}}\right\} \tag{10}$$

where

$$\overline{\alpha^{(k)}} = \sqrt{\frac{3}{2}\alpha_{ij}^{(k)}\alpha_{ij}^{(k)}} \tag{11}$$

$$\overline{\dot{\varepsilon}^{in}} = \sqrt{\frac{2}{3}\dot{\varepsilon}_{ij}^{in}\dot{\varepsilon}_{ij}^{in}} \tag{12}$$

$\zeta^{(k)}$ and $r^{(k)}$ in eq.(10) were constants in the original model but the latter is assumed to change with inelastic strain to describe cyclic hardening, as will be described later. *H(x)* is thr Heaviside function which acts as *H(x)=1* for $x \geqq 0$, and *H(x)*=0 for $x < 0$. $\langle\ \rangle$ is Macauley 's parenthesis operating as <x>=x when $x \geqq 0$ and <x>=0 when $x < 0$.

The first term in the parenthesis of the right-hand side of eq.(10) represents strain hardening whereas the second term gives dynamic recovery to bound the norm of $\alpha_{ij}^{(k)}$ within $\sqrt{2/3}r^{(k)}$. The third term was the one newly added (Ohno and Abdel-Karim, 2000) to allow some ratcheting deformation, even small, and relaxation of mean stress, even slow.

In the uniaxial stress condition, the principal component develops linearly with inelastic strain at the rate of $d\alpha^{(k)}/d\varepsilon_p = \zeta^{(k)} r^{(k)}$ and saturates at $r^{(k)}$ when the third term can be neglected (Fig.1). As a result of this property, uniaxial stress-strain relation is in turn expressed by multi-linear relation. The following relationships can be used to determine the constants.

$$\kappa = \sigma^{(0)} \tag{13}$$

$$\zeta^{(k)} = \frac{1}{\varepsilon_p^{(k)}} \tag{14}$$

$$r^{(k)} = \varepsilon_p^{(k)} \left(\frac{\sigma^{(k)} - \sigma^{(k-1)}}{\varepsilon_p^{(k)} - \varepsilon_p^{(k-1)}} - \frac{\sigma^{(k+1)} - \sigma^{(k)}}{\varepsilon_p^{(k+1)} - \varepsilon_p^{(k)}} \right) \quad \left(k = 1 \sim n-1\right) \tag{15}$$

$$r^{(n)} = \varepsilon_p^{(n)} \frac{\sigma^{(n)} - \sigma^{(n-1)}}{\varepsilon_p^{(n)} - \varepsilon_p^{(n-1)}} \tag{16}$$

where $\sigma^{(k)}$ and $\varepsilon_p^{(k)}$ are stress and plastic strain at the *k*-th intersections of linear segments (see Fig. 2). Particularly, $\sigma^{(0)}$ represents the yield stress corresponding to $\varepsilon_p^{(0)} = 0$. Existence of the third term introduces nonlinearity to each segment but its effect is not large as long as C is relatively small.

2.1.4 Introduction of temperature dependency and property change

Both temperature dependency and the property change by prior loading history are important for simulation capability. To represent both features, the following simple equation is assumed

$$\sigma^{(k)} = \sigma_o^{(k)} + \sigma_h^{(k)} \quad \left(k = 0 \sim n\right) \tag{17}$$

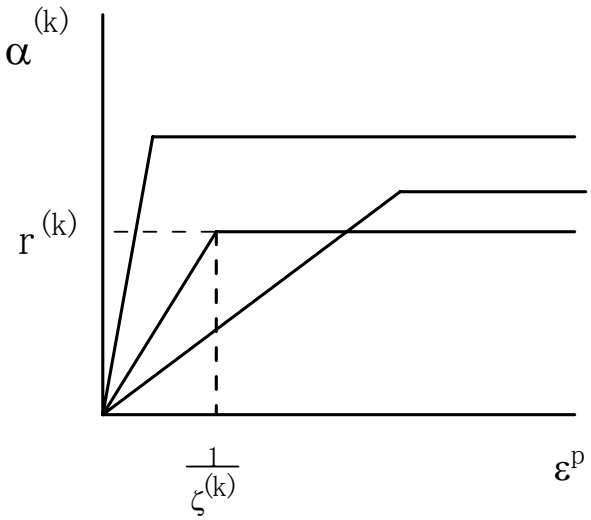

Fig. 1 Change of kinematic hardening parameters with plastic strain

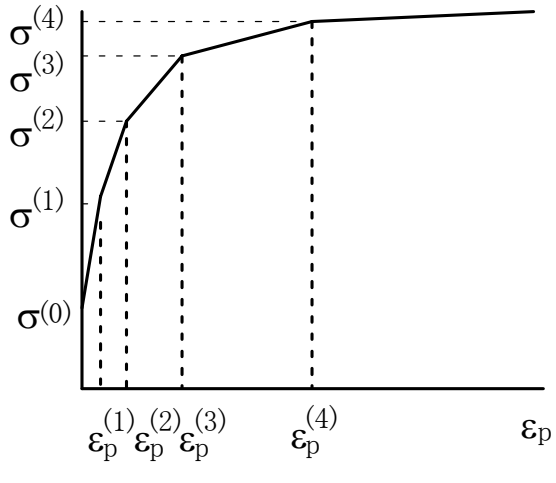

Fig. 2 Multiliear representation of plastic strain – stress relation

where $\sigma_o^{(k)}$ is $\sigma^{(k)}$ at the initial state and is a function of temperature, while $\sigma_h^{(k)}$ represents the amount of hardening dependent on prior loading history material point has experienced. Moreover, $\sigma_h^{(k)}$ is divided into the monotonic and cyclic parts as

$$\sigma_h^{(k)} = \sigma_{mh}^{(k)} + \sigma_{ch}^{(k)} \qquad \left(k = 0 \sim n\right) \tag{18}$$

The monotonic contribution $\sigma_{mh}^{(k)}$ is basically governed by the maximum value of equivalent inelastic strain, allowing some recovery. It is assumed to be 0 initially and develop with the following equation;

$$\dot{\sigma}_{mh}^{(k)} = A_H^{(k)} \dot{\varepsilon}_{\max} + \dot{A}_H^{(k)} \varepsilon_{\max} - A_R \sigma_{mh}^{(k)} \overline{\dot{\varepsilon}^{in}} \tag{19}$$

where $A_H^{(k)}$ and A_R are temperature-dependent constants which determine the rate of hardening and recovery, respectively, whereas $\varepsilon_{\max}$ is the maximum value of $\overline{\varepsilon^{in}}$ defined as

$$\overline{\varepsilon^{in}} = \sqrt{\frac{2}{3}\varepsilon_{ij}^{in}\varepsilon_{ij}^{in}} \tag{20}$$

The cyclic hardening term, $\sigma_{ch}^{(k)}$ is also zero initially and develops as

$$\begin{aligned} \dot{\sigma}_{ch}^{(k)} &= L_H \left\langle \overline{\sigma_{ch}^{(k)}} + \left(\frac{L_R \overline{\sigma_{ch}^{(k)}}}{L_H} \right)^{\frac{1}{n}} - \sigma_{ch}^{(k)} \right\rangle^n \overline{\dot{\varepsilon}^{in}} - L_R \sigma_{ch}^{(k)} \overline{\dot{\varepsilon}^{in}} \quad \text{for } \overline{\sigma_{ch}^{(k)}} \geq 0 \\ &= L_R \left(\overline{\sigma_{ch}^{(k)}} - \sigma_{ch}^{(k)} \right) \overline{\dot{\varepsilon}^{in}} \quad \text{for } \overline{\sigma_{ch}^{(k)}} < 0 \end{aligned} \tag{21}$$

where $\overline{\sigma_{ch}^{(k)}}$ is the asymptotic value for $\sigma_{ch}^{(k)}$ which can be obtained in a way described later, L_H and n are constants to control the rate of cyclic hardening while L_R determines the rate of its recovery.

As a process of obtaining $\overline{\sigma_{ch}^{(k)}}$, the following calculation is made using ρ and temperature, T, at every instance during inelastic deformation process.

.

$$\widetilde{\sigma_{ch}^{(k)}} = H\left(f^{(k)}\left(\rho, T\right) - \widetilde{\sigma_{ch}^{(k)}} \right) \dot{f}^{(k)}\left(\rho, T\right) \tag{22}$$

where $f^{(k)}\left(\rho, T\right)$ is the amount of maximum hardening when the material is cyclically loaded at the inelastic strain range, 2 ρ, and the temperature, *T*.

In addition to that, the following substitutions are applied:

$$\overline{\sigma_{ch}^{(k)}} = \widetilde{\sigma_{ch}^{(k)}} \tag{23}$$

$$\widetilde{\sigma_{ch}^{(k)}} = f^{(k)}\left(0, T\right) \tag{24}$$

at the moment when

$$\nu_{ij} \dot{\varepsilon}_{ij}^{in} < 0 \tag{25}$$

is satisfied. It is expressed by these equations that when $\overline{\sigma_{ch}^{(k)}} > \sigma_{ch}^{(k)}$, $\sigma_{ch}^{(k)}$ approaches to $\overline{\sigma_{ch}^{(k)}}$, which is the maximum value of $f^{(k)}(\rho,T)$ experienced between the second latest load reversal point and the latest one. On the other hand, if $\sigma_{ch}^{(k)} < \sigma_{ch}^{(k)}$, $\sigma_{ch}^{(k)}$ gradually decrease towards $\sigma_{ch}^{(k)}$.

2.1.5 Material constants for 316FR

During the process of development of structural design guide, equations for describing monotonic and cyclic stress-strain curves for 316FR were developed as a function of temperature (Japan Atomic Power Company, 1999, Aoto et al., 1995). They were utilized to determine standard material constants involved in the current model, although additional assumptions and formulation were required to fix the details of the model.

The model contains adjustment parameter, κ, to cope with heat-to-heat variation of the material. $\kappa = 1.0$ corresponds to average material property whereas the lower bound property is generated by setting $\kappa = 0.78$, as shown in Figs. 3 and 4..

Table 1 Standard material constants for 316FR (T: temperature in ℃)

$$\sigma_0^{(k)} = \kappa\left\{\sigma_y - K(0.002)^m + K\left(\varepsilon_p^{(k)}\right)^m - A_H^{(k)}\varepsilon_p^{(k)}\right\} \quad for \quad \varepsilon_p^{(k)} \le 0.01$$

$$\sigma_0^{(k)} = \kappa\left\{\sigma_y - K(0.002)^m + K(0.01)^m + \frac{K\left[(0.025)^m - (0.01)^m\right]}{0.015}\left(\varepsilon_p^{(k)} - 0.01\right) - A_H^{(k)}\varepsilon_p^{(k)}\right\}$$

$$for \quad \varepsilon_p^{(k)} > 0.01$$

$$A_H^{(k)} = \frac{0.95K\left[(0.025)^m - (0.01)^m\right]}{0.015}$$

$$\sigma_y = 273.364 - 0.740603T + 0.00138828T^2 - 0.000000908682\,T^3$$

$$K = 399.777 - 0.0580824\,T$$

$$m = 0.205730 + 0.000138879\,T$$

$$f^0(\rho,T) = \kappa\left(-49.47 + 0.020695\,T + 0.000024247\,T^2 + 0.00000032022\,T^3\right)$$

$$f^{(k)}(\rho,T) = \underset{p=1,k}{Max}\left\{f^{(0)}(T), g^{(p)}(\rho,T)\right\}$$

$$g^{(k)}(\rho,T) = f^{(0)}(T) + \kappa\left\{\frac{1 - 0.0002946\left[\min(\varepsilon_p^{(k)},\rho) + 0.0001312\right]^{-0.9095}}{1 - 0.0002946\left[\rho + 0.0001312\right]^{-0.9095}}\left[10^a(2\rho)^{m_d} - K\rho^m - \frac{f^{(0)}(T)}{\kappa}\right]\right\}$$

$$a = 3.97220 - 0.00313844T + 0.00000476051T^2 - 0.00000000249678T^3$$

$$m_d = 0.819459 - 0.000755358\,T - 0.0000009457534\,T^2 + 0.00000000194329\,T^3$$

$$C = 0.05$$

$$A_R = 10$$

$$L_H = 0.0025$$

$$n = 2.5$$

$$L_R = 0.5$$

k	0	1	2	3	4	5	6
$\varepsilon_p^{(k)}$	0	0.0001	0.0002	0.0003	0.0005	0.00075	0.001

7	8	9	10	11	12	13	14
0.0015	0.002	0.003	0.004	0.006	0.008	0.01	0.1

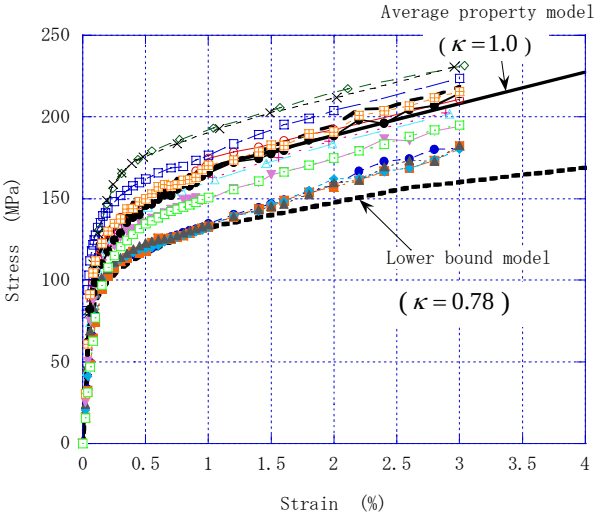

Fig. 3 Comparison of model prediction and test data on monotonic stress-strain curve (550℃)

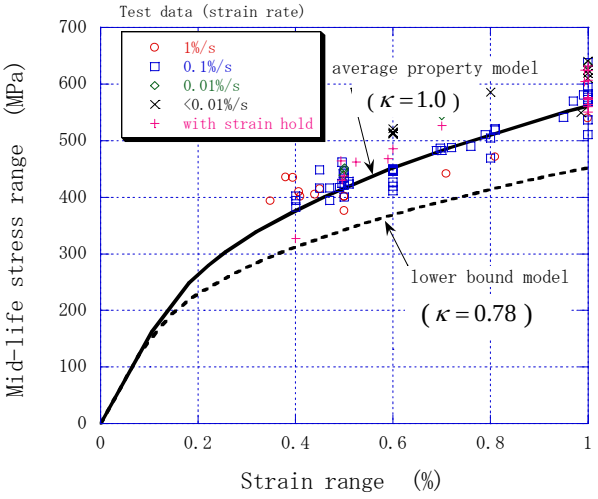

Fig. 4 Comparison of model prediction and test data on cyclic stress-strain curve (550℃)

2.2 Model for Creep Analysis

2.2.1 Creep hardening index surface

In similar to the plastic hardening index surface described above, creep hardening index surface is defined by (Murakami and Ohno, 1982)

$$g_c = \frac{2}{3}\left(\varepsilon_{ij}^c - \beta_{ij}^c\right)\left(\varepsilon_{ij}^c - \beta_{ij}^c\right) - \rho_c^2 = 0 \tag{26}$$

where ε_{ij}^c is creep strain whereas β_{ij}^c and $\sqrt{3/2}\rho_c$ represent the shift and size of the surface, respectively. All components of β_{ij}^c as well as ρ_c are 0 at the initial state but change with creep deformation according to.

(i) when $g_c = 0$ and $\left(\varepsilon_{ij}^c - \beta_{ij}^c\right)\dot{\varepsilon}_{ij}^c > 0$,

$$\dot{\beta}_{ij}^c = (1-\lambda)\dot{\varepsilon}_{kl}^c n_{kl} n_{ij} \tag{27}$$

$$\dot{\rho}_c = \sqrt{2/3}\lambda\dot{\varepsilon}_{ij}^c n_{ij} \tag{28}$$

(ii) when $g_c < 0$ or $\left(\varepsilon_{ij}^c - \beta_{ij}^c\right)\dot{\varepsilon}_{ij}^c \le 0$

$$\dot{\beta}_{ij}^c = 0 \tag{29}$$

$$\dot{\rho}_c = 0 \tag{30}$$

where n_{ij} represents the normal outward to the creep hardening surface calculated by

$$n_{ij} = \frac{\varepsilon_{ij}^c - \beta_{ij}^c}{\sqrt{(\varepsilon_{kl}^c - \beta_{kl}^c)(\varepsilon_{kl}^c - \beta_{kl}^c)}} \tag{31}$$

λ in eqs.(27-28) represents the ratio of shift and expansion of the surface and is assumed to be 0.5.

To represent the recovery of hardening due to reversed plastic loading, it is assumed that β_{ij}^c and ρ_c also change when the plastic strain is generated according to the following equations (Takahashi et al., 2001):

(i) when $g_c = 0$ and $\left(\varepsilon_{ij}^c - \beta_{ij}^c\right)\dot{\varepsilon}_{ij}^p > 0$,

$$\dot{\beta}_{ij}^c = 0 \tag{32}$$

$$\dot{\rho}_c = 0 \tag{33}$$

(ii) when $g_c = 0$ and $\left(\varepsilon_{ij}^c - \beta_{ij}^c\right)\dot{\varepsilon}_{ij}^p < 0$,

$$\dot{\beta}_{ij}^c = -\lambda_p \dot{\varepsilon}_{kl}^p n_{kl} n_{ij} \tag{34}$$

$$\dot{\rho}_c = \sqrt{2/3}\lambda_p \dot{\varepsilon}_{ij}^p n_{ij} \tag{35}$$

(iii) when $g_c < 0$,

$$\dot{\beta}_{ij}^c = -\lambda_p \dot{\varepsilon}_{ij}^p \tag{36}$$

$$\dot{\rho}_c = -\lambda_p \sqrt{\frac{2}{3}\dot{\varepsilon}_{ij}^p \dot{\varepsilon}_{ij}^p} \tag{37}$$

where λ_p represents the degree of recovery of creep hardening and is assumed to be 0.5.

2.2.2 Flow rule

β_{ij}^c and ρ_c developed according to those equations are used to obtain the equivalent creep strain as

$$q = \frac{1}{2\lambda}\{\rho_c + \frac{\left(\varepsilon_{ij}^c - \beta_{ij}^c\right)s_{ij}}{\sqrt{(3/2)s_{kl}s_{kl}}}\} \tag{38}$$

and then q is used to obtain equivalent time, t_e and finally equivalent creep strain rate in uniaxial constant-stress creep strain equation such as given in (Japan Atomic Power Company, 1999).

Finally creep strain rate is calculated by

$$\dot{\varepsilon}_{ij}^c = \frac{3}{2}\frac{\overline{\dot{\varepsilon}^c}}{\bar{\sigma}}s_{ij} \tag{39}$$

using the equivalent stress, $\bar{\sigma}$ and equivalent creep strain, $\overline{\dot{\varepsilon}^c}$, defined as

$$\bar{\sigma} = \sqrt{\frac{3}{2}s_{ij}s_{ij}} \tag{40}$$

$$\overline{\dot{\varepsilon}^c} = \sqrt{\frac{2}{3}\dot{\varepsilon}_{ij}^c \dot{\varepsilon}_{ij}^c} \tag{41}$$

3. EVALUATION OF SIMULATION CAPABILITY

Many calculations have been conducted to evaluate the capability of the model via comparison with experimental data. Principal comparison was made on the deformation data in standard strain-controlled fatigue tests and predictions by the model corresponding to average property. Both changes of peak stresses with cycles and steady-state hysteresis loops were compared at several temperatures and several strain ranges. Typical examples are shown in Figs. 5 and 6. Reasonable agreements between the test data and simulations can be seen in the variation of peak stress and steady-state hysteresis loop, although some difference on the hysteresis loop appears at relatively high strain ranges.

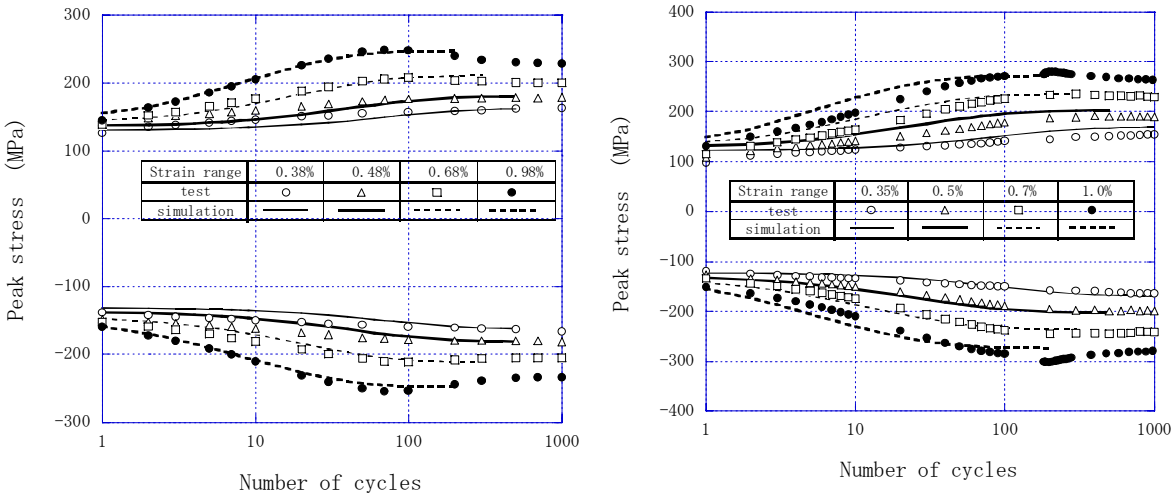

(a) 400℃ (b) 550℃

Fig. 5 Comparison of test data and simulation on the variation of peak stress in iso-thermal fatigue test

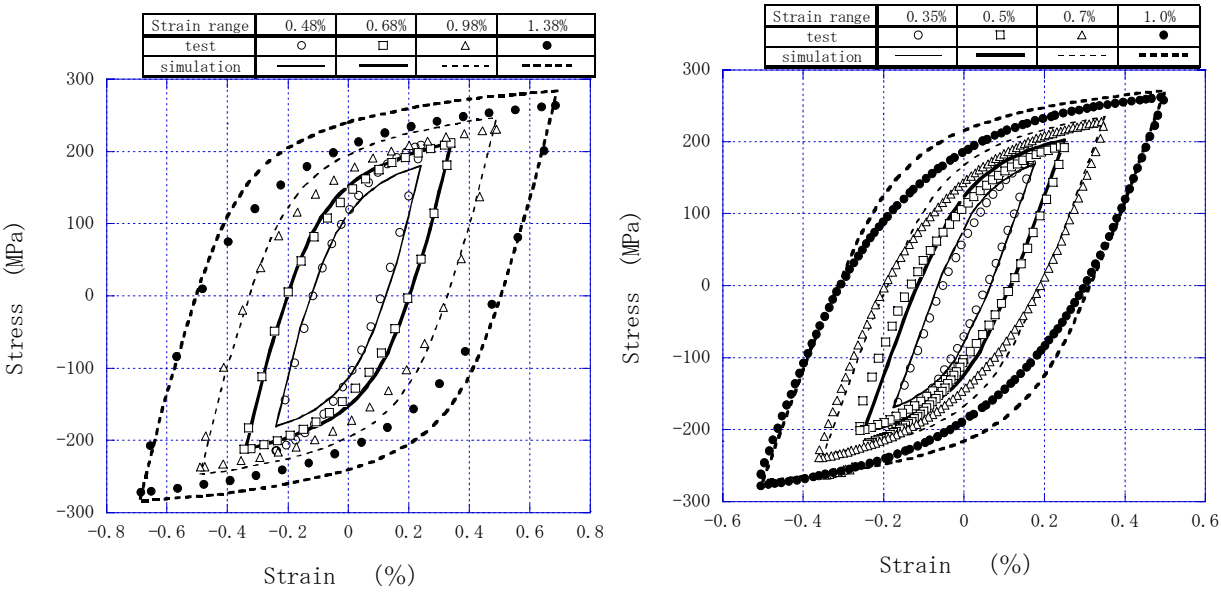

(a) 400℃ (b) 550℃

Fig. 6 Comparison of test data and simulation on the steady-state hysteresis loops in iso-thermal fatigue test

To ensure the applicability of the model to thermo-mechanical fatigue, several calculations were conducted. Typical examples are shown in Fig. 7. Simulations are in good agreement with the test results similarly to iso-thermal fatigue cases.

Simulation capability of the model under unconventional cyclic loading was also studied. In the existence of asymmetry in strain path, mean stress develops with mean strain but relaxes after the mean strain is fixed. The new model can predict these behaviors observed under the constant and progressive mean strain with a reasonably accuracy as shown in Figs. 8 and 9, in contrast to large deviation of the previous model.

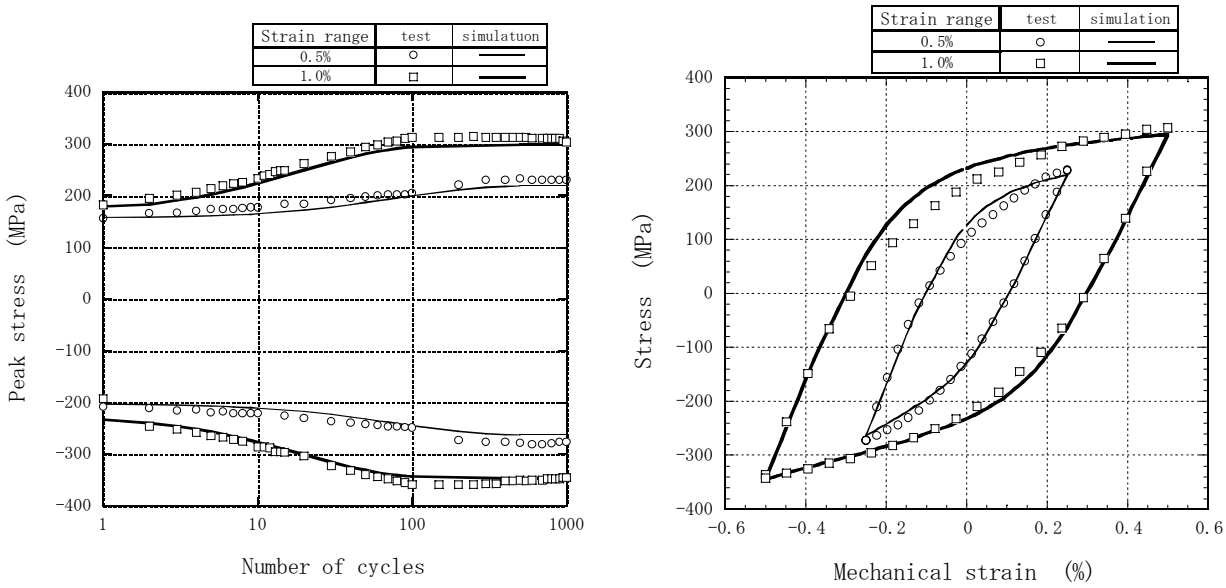

(a) Variation of peak stresses with cycles

(b) Steady-state hysteresis loops

Fig. 7 Comparison of test data and simulations in thermo-mechanical fatigue tests (200℃-550℃, in-phase)

4. CONCLUSION

Inelastic constitutive model was developed to simulate cyclic deformation behavior of austenitic stainless steel with a sufficient accuracy for design application. Standard material constants were derived for 316FR steel with an adjustment parameter for heat-to-heat variation. The model was proven to have sufficient capability to simulate cyclic deformation behavior both under the absence and presence of the mean strain. Applicability to thermo-mechanical loading was also demonstrated.

This study was conducted as a part of "Study on Verification of Advanced Power Reactor Technologies," which was promoted by Japan Atomic Power Company under the sponsorship of the Ministry of Economy, Trade and Industry.

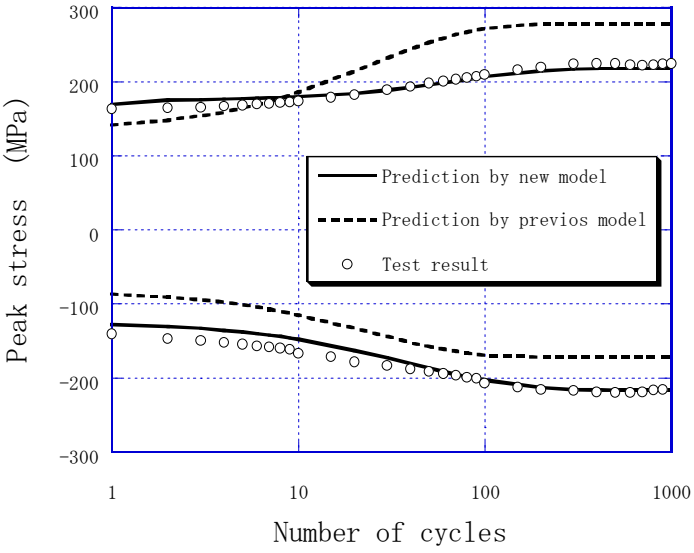

Fig. 8 Variation of peak stress under cyclic loading with constant mean strain (550℃, strain range : 0.5%, mean strain : 1.0%)

REFERENCES

[1] Aoto, K., Iwata, K. and Wada, Y., (1995), presented at 5th Int. Symp. on Plasticity and Its Current Application.
[2] Armstrong, P. J. and Frederick, C. O., (1966) CEGB Report RD/B/N731.
[3] Chaboche, J. L. and Rousselier, G., (1983), Trans. ASME J. Press, Vessel Technol., Vol. 105, p. 153.

[4] Japan Atomic Power Company, (1999), High-temperature Structural Design Standard for Demonstration Fast Breeder Reactor (draft, in Japanese).
[5] Murakami, S. and Ohno, N., (1982), Int. J. Solids Struct., Vol. 18, p. 597.
[6] Ohno, N. and Wang, J. D., (1993), Int. J. Plasticity, Vol. 9, p. 375.
[7] Ohno, N. and Wang, J. D., (1993), Int. J. Plasticity, Vol. 9, p. 391.
[8] Ohno, N. and Abdel-Karim, M., (2000), ASME, J. Eng. Mater. Technol., Vol. 122, p/ 35.
[9] Pugh, C. E., (1983), Trans. ASME J. Press, Vessel Technol., Vol. 105, p. 273.
[10] Takahashi, Y., (1993), ASME PVP-Vol.262, p. 201.
[11] Takahashi, Y. and Tanimoto, K., (1995), Trans. 13th SMiRT, Col. 1, p. 427.
[12] Takahashi, Y., (1998), ASME Book No. H01146, p. 167.
[13] Takahashi, Y., Ohno, N. and Yagawa, G., (2001), 16th SMiRT, paper No. 1426.

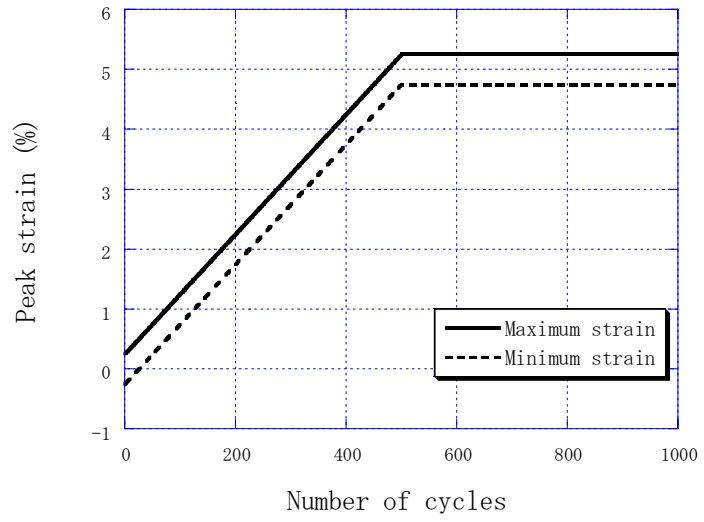

(a) Change of peak strain with cycles

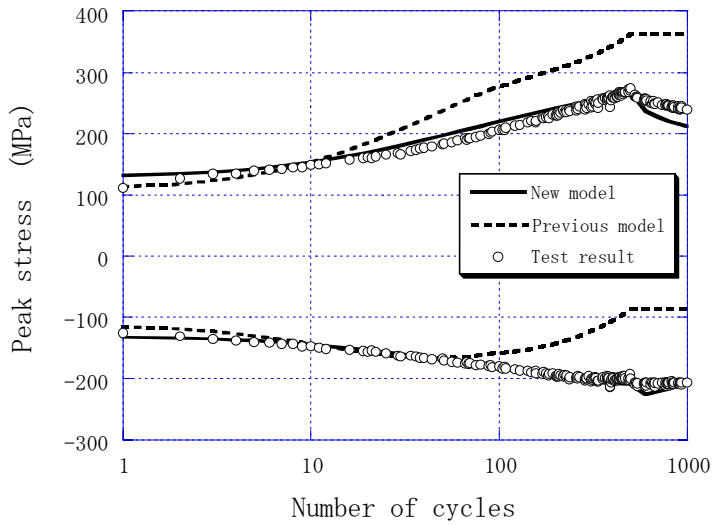

(b) Change of peak stress with cycles

Fig. 9 Variation of peak stress under cyclic loading with progressive mean strain (550℃, strain range : 0.5%, mean strain : 0-5.0%)

